

Experimental demonstration of particle acceleration with normal conducting accelerating structure at cryogenic temperature

Mamdouh Nasr,^{1,*} Emilio Nanni,¹ Martin Breidenbach,¹ Stephen Weathersby,¹ Marco Oriunno,¹ and Sami Tantawi¹

¹*SLAC National Accelerator Laboratory, 94025 California, USA*

Abstract: Reducing the operating temperature of normal conducting particle accelerators substantially increases their efficiency. Low-temperature operation increases the yield strength of the accelerator material and reduces surface resistance, hence a great reduction in cyclic fatigue could be achieved resulting in a large reduction in breakdown rates compared to room-temperature operation. Furthermore, temperature reduction increases the intrinsic quality factor of the accelerating cavities, and consequently, the shunt impedance leading to increased system efficiency and beam loading capabilities. In this paper, we present an experimental demonstration of the high-gradient operation of an X-band, 11.424 GHz, 20-cells linear accelerator (linac) operating at a liquid nitrogen temperature of 77 K. The tested linac was previously processed and tested at room temperature. We verified the enhanced accelerating parameters of the tested accelerator at cryogenic temperature using different measurements including electron beam acceleration up to a gradient of 150 MV/m, corresponding to a peak surface electric field of 375 MV/m. We also measured the breakdown rates in the tested structure showing a reduction of two orders of magnitude, $\times 100$, compared to their values at room temperature for the same accelerating gradient.

The operation of particle accelerators at high-gradient levels is essential in future discovery machines for particle colliders and free-electron lasers as well as advanced medical applications [1–4]. The accelerating gradient is defined as the energy gained by a charged particle moving along the axis of the accelerating structure per unit length, in eV/m. Normal conducting (NC) accelerating structures have been a leading candidate in high-gradient acceleration, with an accelerating gradient above 100 MV/m, for their capability of sustaining higher surface fields compared to their superconducting counterparts [5]. The demanding applications for high-gradient operation and more compact machines derive a continuous international effort to push the boundaries of particle accelerator technology by providing compact accelerating structures with optimized geometries and enhanced accelerating properties.

A limiting factor in the operation of high-gradient accelerating structures is the rf breakdowns on the surface which cause vacuum arcs that can perturb acceleration [6]. Consequently, a critical parameter in defining the operation of high-gradient accelerators is the rf breakdown rates at the accelerating gradient of interest. Studies have shown that breakdown rates are largely correlated to the peak electric and magnetic fields on the surface and might be explained by the movement of crystal defects due to the surface stress from peak pulsed heating as well as the high electric field on the inner accelerator surface [7–10]. There has been an effort to minimize the breakdown rates in high-gradient accelerators by building accelerator structures from harder materials, which showed lower breakdown rates compared to the ones built from softer materials [11, 12].

Another approach that was experimentally investigated to enhance the operation of NC accelerators is by operation at cryogenic temperatures which substan-

tially reduces the surface-resistance compared to room-temperature operation. This reduction increases the shunt impedance and intrinsic quality factor of the accelerating cavities leading to increased system efficiency and beam loading capabilities; The shunt impedance is defined as the square of the accelerating gradient divided by the power loss per unit length of the accelerating structure, in Ω/m . Moreover, low-temperature operation increases surface hardness [13] which is expected to largely reduce the breakdown rates compared to room-temperature operation for the same accelerating gradient.

Few experiments investigated the operation of NC accelerating cavities at cryogenic temperatures. In [14], the operation of accelerating cavities at 3 GHz and liquid nitrogen (LN) temperature of 77 K was investigated. The experiment showed excessive deterioration in the intrinsic quality factor for surface electric fields higher than 150 MV/m. The authors concluded that this degradation is caused by the high rf magnetic field on the surface. Other studies were performed at low-gradient levels, below 50 MV/m [15, 16]. These experiments verified the intrinsic quality factor of the tested cavities at cryogenic temperatures. However, they did not demonstrate high-gradient operation or study the breakdown rates in the tested structures. An investigation performed by CERN studied the breakdown rates for a set of cavities with frequencies between 21 and 35 GHz at operating temperatures between 100 and 800 K [17]. The study showed no dependence of the breakdown rates on the temperature of operation.

A recent experimental effort aimed to provide a more elaborate picture of the operation of high-gradient accelerating cavities at cryogenic temperature [18]. The authors performed an experimental investigation on a single-cell accelerating structure at 11.424 GHz and 45

K. They reported reduced breakdown rates at cryogenic temperatures compared to room temperature operation. This reduction enabled reaching an accelerating gradient of 250 MV/m. They also reported a time-dependent degradation in the intrinsic quality factor of the accelerating cavity for accelerating gradients higher than 150 MV/m [19]. The experiments observed the onset of breakdowns at an accelerating gradient of 250 MV/m, but were unable to characterize the breakdown probability's dependence on accelerating gradient with the collected statistics.

The experimental effort in [14–16, 18, 19] showed a large promise in the operation of NC accelerators at cryogenic temperatures for enhanced shunt impedance and reduced breakdown rates. This effort was performed, however, for single-cell testing and/or low-gradient operation, below 50 MV/m. Also, the lack of defined slopes for the breakdown rates versus the accelerating gradient at cryogenic temperature does not provide a clear understanding of the statistical behavior of breakdown rates. Most importantly, these experiments did not attempt to demonstrate particle acceleration with the tested structures. To the best of the authors' knowledge, there has never been an experimental demonstration of the operation of multi-cell NC accelerating structures at cryogenic temperature and high-gradient levels.

In our work, we develop a practical approach and methodology for the high-gradient operation of multi-cell NC accelerating structures at cryogenic temperature. This development is a necessary milestone in the road of adapting Cryogenic-NC-accelerators in many practical applications including future discovery machines. Practical and economic aspects are thus important. We decided to operate at a cryogenic temperature of LN of 77 K. Operating with the LN cooling system results in much-reduced system cost compared to the complicated setup required for the operation with LHe, and still provides much-enhanced accelerating parameters compared to room temperature operation. We verified the accelerating parameters using many approaches including energy-gain measurements with electron-beam. We also performed an extensive study on the breakdown rates for the same accelerator structure at room and cryogenic temperatures.

The rf surface resistance of good-conductors at cryogenic temperatures is well studied and explained using the theory of anomalous skin effect (ASE) [20]. At low temperatures and high frequencies, the mean free path of electrons becomes comparable or larger than the classical skin depth for good conductors. In this case, the electrons that contribute the most to the current are the ones that spend their entire mean free path in the skin depth, and the surface resistance saturates to a higher value than the one predicted by the classical skin depth. Fig. 1 shows the surface resistance for copper (RRR=400) versus temperature at 11.424 GHz. In our calculations, we

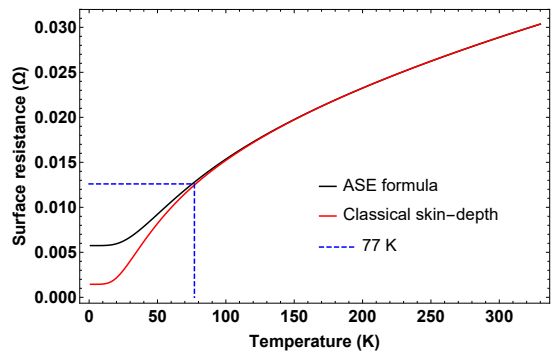


FIG. 1. At low temperatures the surface resistance, predicted by ASE, saturates to higher values than the ones calculated from the classical skin depth. Operating at 77 K results in a reduction in the surface resistance of a factor of 2.25 compared to 300 K.

used the Bloch-Grüneisen Formula in [21] to calculate the bulk conductivity versus temperature, and the equations for the ASE in the simplified form presented in [22]. At low temperatures, the surface resistance, predicted by the ASE, saturates to higher values than the ones calculated from the classical skin depth. Operating at 77 K results in a reduction in the surface resistance of a factor of 2.25 compared to 300 K.

We tested an X-band, 11.424 GHz, 20-cells, standing-wave linear accelerator (linac) structure which has been previously processed and tested at room temperature up to a gradient of 140 MV/m [23]. Table I shows the tested linac parameters at 300 K and 77 K. We modified the existing setup at X-band Test Accelerator (XTA) station at the NLCTA facility at SLAC to accommodate high-power experiments at cryogenic temperatures. The experimental setup is shown in Fig. 2(a). XTA is divided into two stations, referenced in Fig. 2(a) as stations 1 and 2; Each station is fed with an independent rf source. The first station is used to generate the electron beam from an X-band photoinjector and then accelerate the beam to about 46 MeV, in our experiment, using an NLC style X-band accelerator [24]. The second station feeds the tested linac, which is installed after the station 1 linac. An X-band klystron feeds the accelerator under testing with rf power. The peak rf power of the klystron is 40 MW, and we installed a pulse compressor (multimoded SLED-II [25]) after the klystron to push the rf power above the klystron limit. Quadrupoles are used for beam focusing and trajectory adjustment, a spectrometer is placed after the distributed-coupling linac to measure the beam energy, and a Faraday cup (FC) is installed downstream for charge measurements. We placed a dark-current detector downstream from the tested accelerator to detect dark-current spikes and count the breakdown rates in our tested accelerator.

Figure 2(b) illustrates the cooling system used for our cryogenic experiment. We drilled a hole through the

TABLE I. Summary of the accelerating parameters of the tested accelerating structure at 300 and 77 K. The peak fields are calculated for average accelerating gradient of 100 MV/m.

| Parameter | 300 K | 77 K |
|---------------------------------|--------|--------|
| Frequency (GHz) | 11.402 | 11.438 |
| Q_0 | 10000 | 22500 |
| Q_{ext} | 10000 | 10000 |
| Shunt impedance (M Ω /m) | 155 | 349 |
| Peak surface E (MV/m) | 250 | 250 |
| Peak surface H (MA/m) | 0.575 | 0.575 |
| Iris diameter (mm) | 2.6 | 2.6 |
| Length (cm) | 26 | 26 |

tunnel wall, perpendicular to the beam axis. A foam-insulated stainless-steel line delivers LN from Dewars outside the tunnel to the cryostat, where the tested linac is sitting inside. A level detector is inserted inside the cryostat and provides a control signal to a solenoid that controls the flow of the LN in the feed line. A vent-out line transports the boiled LN outside the tunnel. The used cryostat is a simple cylindrical stainless-steel container with insulation foam from the outside. The linac structure is sitting inside the cryostat on two half-circular supports with a rectangular opening for the structure to set inside. The cryostat and the linac share the same beam axis and there are two transport tubes under-vacuum from both sides of the linac to the cryostat walls perpendicular to the beamline. The cryostat has an opening for the feed lines of the LN and the input rf power, and small openings for the LN level detector and vent-out line.

Before installing the cryostat in the beamline, we performed a cold-test of our accelerator structure at the cryogenic temperature of LN. We installed the accelerator structure, under-vacuum, inside the cryostat, and used LN Dewar to supply LN directly into the cryostat. A VNA was connected to the rf input of the structure, through a vacuum window, to measure the reflection coefficient at the rf input port to the accelerator. Figure 3 shows the reflection coefficient at the rf input to the accelerator at 300 K and 77 K. As the accelerator structure cools down, it shrinks, and thus the resonance frequency shifts to a higher value. We measured a resonance shift of 36 MHz from 300 K to 77 K which is in very good agreement with the calculated value using the thermal expansion of copper [26]. The distributed-coupling linac is designed for critical-coupling at 300 K and becomes over-coupled at 77 K because of the reduced surface resistance which increases the intrinsic quality factor, Q_0 , of the accelerating cavity. Note that the external quality factor remains constant because of the minimal effect of the temperature change on the power-coupling irises to the accelerating cells. We should emphasize that the increase of the coupling coefficient, $\beta = Q_0/Q_e$, for the accelerating structure from 1 to 2.25 from 300 to 77 K

represents a large increase in the beam-loading capability for the same accelerator structure just by cooling it down to cryogenic temperature.

We did another test to measure the change in the quality factor and resonance frequency for the accelerator structure versus temperature. We supplied LN into the cryostat until the structure temperature stabilized. We then stopped the LN supply and measured the reflection coefficient as the structure warms-up to room temperature. Figure 4 shows the measured intrinsic quality factor of the accelerating structure versus resonance frequency from 300 to 67 K. The measured values of the intrinsic quality factor are obtained using Q-circle fitting of the measured reflection coefficient at the rf input port [27]. We compared the measured values of the intrinsic quality factor with our simulations, represented by the dashed line in Fig. 4. In our simulations, we calculated the temperature at each point from the measured shift of the resonance frequency, from its value at room temperature, and the thermal expansion coefficient of copper [26]. We then used the temperature value to calculate the surface resistance using the theory of ASE, previously presented in Fig. 1. The obtained surface resistance is used to simulate the intrinsic quality factor of the accelerator structure. The results show very good agreement between the measurement and simulation. The lowest measured temperature is 67 K, however, for high-power operation, the temperature stabilizes at 77 K with an intrinsic quality factor of 22500.

After verifying the quality factor of our accelerating structure at low-level rf, we installed the cryostat in the XTA beamline. The goal of our experiment is to verify the accelerating parameters of our structure and to collect breakdown statistics for high-power operation at 77 K. We measured the energy gain of an electron beam moving down the axis of the tested linac and compared the results with our simulations using the measured input pulse to the structure and the cavity model, substituting with the accelerating parameters from Table I at 77 K [28]. We performed a set of measurements using a compressed 200 ns square rf pulse with an input power of 13-33 MW achieving an accelerating gradient from 100-150 MV/m, and a peak surface electric field of 250-375 MV/m. Figure 5, shows the measured energy gain versus input rf power showing very good agreement between the measurements and simulations, less than 4% deviation.

Figure. 6 shows the collected breakdown rates, with the fitted slope, for the tested accelerator structure at 77 K with an accelerating gradient of 110-130 MV/m. The breakdown rates are compared with the results from our previous testing of the same accelerator structure at 300 K. For both operating temperatures, the data was collected for a 400 ns stepped pulse with a flat gradient of 200 ns. The results show a reduction of two orders of magnitude, $\times 100$, in breakdown rates at the same gradient levels from 300 to 77 K operation. We believe that

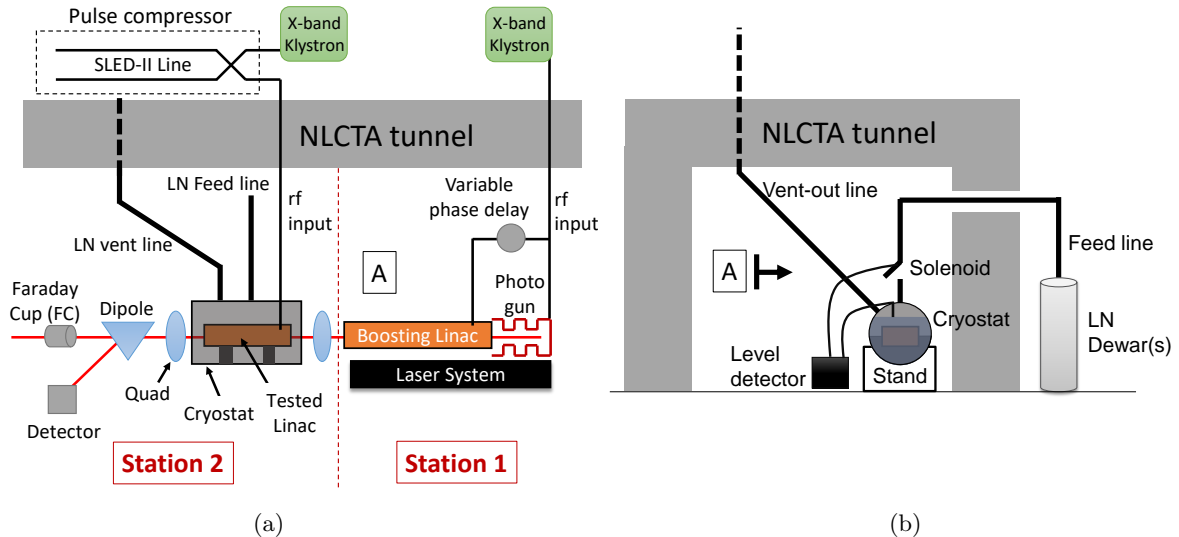


FIG. 2. (a) The experimental setup for accelerator testing at XTA facility at SLAC. XTA is divided into two stations, referenced as station 1 and station 2. The first station generates the electron beam used in the experiment, and the tested accelerator is installed in the second station. (b) A foam-insulated stainless-steel line delivers LN from Dewars outside the tunnel to the cryostat where the tested linac is setting inside, through a hole in the tunnel wall. A level detector is inserted inside the cryostat and provides a control signal to a solenoid that controls the flow of the LN in the feed line. A vent-out line transport the boiled LN outside the tunnel.

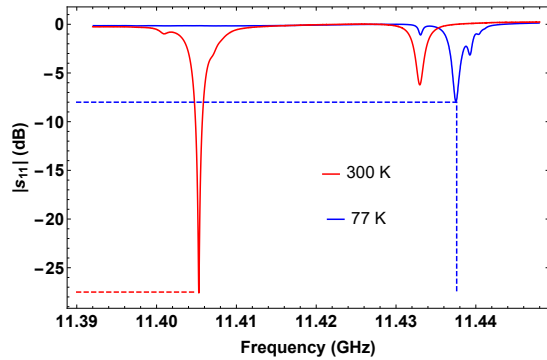


FIG. 3. The reflection coefficient at the rf input to the accelerator at 300 K and 77 K. As the accelerator structure cools down, it shrinks leading to a shift of the resonance frequency of 36 MHz. The tested linac is designed for critical-coupling at 300 K, $|s_{11}| = -27$ dB at resonance, and becomes over-coupled at 77 K, $|s_{11}| = -8$ dB at resonance, because of the reduced surface resistance which increases the intrinsic quality factor of the accelerating cavity while the external one remains constant.

this reduction in breakdown rates is correlated to the increased hardness of copper at cryogenic temperature. This reduction and the observed increase in the slopes of the breakdown lines at 77 K is in agreement with the previously observed behavior for accelerating cavities built with hard versus soft copper [11, 12]. The results are also in agreement with the reduced breakdown rates reported in [18]. Our results provide comprehensive breakdown statistics for the high-gradient operation of NC accelera-

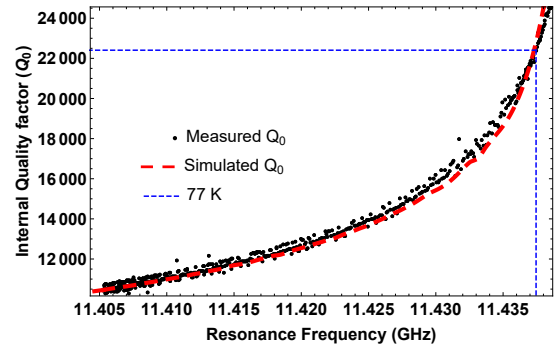


FIG. 4. The intrinsic quality factor of the accelerating structure versus the resonance frequency. Black dots and dashed-line are the measured and simulated values, respectively. The measured values are obtained using Q-circle fitting of the measured reflection coefficient at the rf input port. In our simulations, the temperature at each point is used to calculate the surface resistance using the theory of ASE and simulate the intrinsic quality factor.

tors at cryogenic temperature. These results give a more realistic intuition on the dependence of breakdown rates on the operating temperature compared to the study in [17] that showed no temperature dependence of the breakdown rates in the tested cavities. This reduction in breakdown rates at lower temperatures of operation is also predicted using different proposed breakdown models for normal conducting accelerating structures [7–10].

The presented experiment provides the first demonstration of high-gradient acceleration of an electron-beam

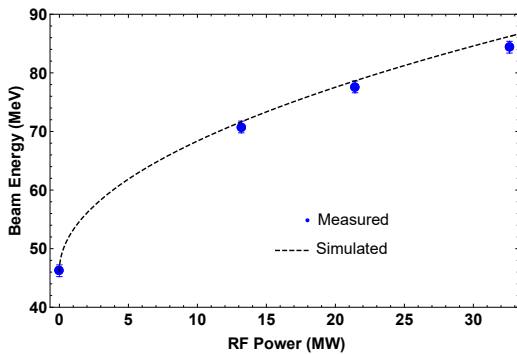


FIG. 5. The measured energy gain of an electron beam moving down the axis of the tested linac for a compressed 200 ns square rf pulse with input power of 13-33 MW achieving accelerating gradient from of 100-150 MV/m, and peak surface electric field of 250-375 MV/m. Blue dots and dashed-line are the measured and simulated values, respectively. Simulations used the measured input rf pulse to the structure and the cavity model to calculate the energy gain at 77 K.

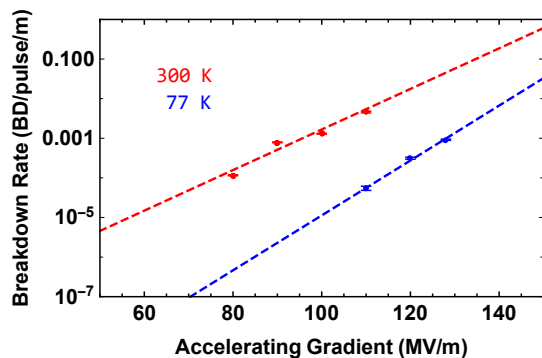


FIG. 6. The collected breakdown rates, with the fitted slope, of the tested accelerator structure at 300 and 77 K. The breakdown rates at 300 K are obtained from our previous testing of the same accelerator structure at room temperature [23]. The results show a reduction of two orders of magnitude, $\times 100$, in breakdown rates at the same gradient levels from 300 to 77 K operation.

at a cryogenic temperature of 77 K; We reached a gradient level of 150 MV/m with a peak surface electric field of 375 MV/m. The structure achieved a shunt impedance of 349 M Ω /m and $\times 2.25$ enhancement in the beam loading capabilities compared to 300 K operation. The experiment provides a practical and cost-effective approach for the high-gradient operation of NC accelerators at cryogenic temperatures of 77 K with LN cooling. We presented a comprehensive breakdown study of the tested accelerator structure at cryogenic temperature and high-gradient operation showing two orders of magnitude, $\times 100$, reduction in breakdown rates from 300 to 77 K. The reduced breakdown rates agree with our understanding of the correlation between reduced breakdown rates and the increased material hardness. This experimental investigation provides a critical milestone

for the practical use of NC accelerating systems at cryogenic temperatures which motivates many proposals for future discovery machines with optimized cost and performance parameters [29–31].

* Corresponding author: mamdouh@slac.stanford.edu

- [1] C. Adolphsen, *The International Linear Collider Technical Design Report-Volume 3. II: Accelerator Baseline Design*, Tech. Rep. (Argonne National Lab.(ANL), Argonne, IL (United States); Thomas Jefferson, 2013).
- [2] T. CLIC, T. Charles, P. Giansiracusa, T. Lucas, R. Rasool, M. Volpi, C. Balazs, K. Afanaciev, V. Makarenko, A. Patapenka, *et al.*, arXiv preprint arXiv:1812.06018 (2018).
- [3] B. W. McNeil and N. R. Thompson, *Nature photonics* **4**, 814 (2010).
- [4] K. Kokurewicz, E. Brunetti, G. H. Welsh, S. Wiggins, M. Boyd, A. Sorensen, A. Chalmers, G. Schettino, A. Subiel, C. DesRosiers, *et al.*, *Scientific reports* **9**, 1 (2019).
- [5] N. Solyak, in *AIP Conference Proceedings*, Vol. 1086 (American Institute of Physics, 2009) pp. 365–372.
- [6] H. Timko, F. Djurabekova, K. Nordlund, L. Costelle, K. Matyash, R. Schneider, A. Toerklep, G. Arnau-Izquierdo, A. Descoeudres, S. Calatroni, M. Taborelli, and W. Wuensch, *Phys. Rev. B* **81**, 184109 (2010).
- [7] A. Grudiev, S. Calatroni, and W. Wuensch, *Physical Review Special Topics-Accelerators and Beams* **12**, 102001 (2009).
- [8] K. Nordlund and F. Djurabekova, *Physical Review Special Topics-Accelerators and Beams* **15**, 071002 (2012).
- [9] V. A. Dolgashev, in *Proceedings of the 2003 Particle Accelerator Conference*, Vol. 2 (IEEE, 2003) pp. 1267–1269.
- [10] L. Laurent, S. Tantawi, V. Dolgashev, C. Nantista, Y. Higashi, M. Aicheler, S. Heikkinen, and W. Wuensch, *Physical review special topics-accelerators and beams* **14**, 041001 (2011).
- [11] V. A. Dolgashev, in *AIP Conference Proceedings*, Vol. 1507 (American Institute of Physics, 2012) pp. 76–84.
- [12] V. Dolgashev *et al.*, in *2nd European Advanced Accelerator Concepts Workshop (EAAC 2015), La Biodola, Isola d’Elba, Italy* (2015) pp. 13–19.
- [13] R. P. Reed and R. P. Mikesell, (1967).
- [14] A. McEuen, P. Lui, E. Tanabe, and V. Vaguine, *IEEE Transactions on Nuclear Science* **32**, 2972 (1985).
- [15] A. Saversky and I. Shchedrin, in *Proceedings of International Conference on Particle Accelerators* (IEEE, 1993) pp. 1030–1032.
- [16] A. Iino, S. Yamaguchi, T. Higo, S. Michizono, T. Shintomi, Y. Funahashi, S. Matsumoto, J. Endo, and K. Ueno, (2016).
- [17] H. H. Braun, S. Döbert, I. Wilson, and W. Wuensch, *Physical review letters* **90**, 224801 (2003).
- [18] A. Cahill, J. Rosenzweig, V. A. Dolgashev, S. G. Tantawi, and S. Weathersby, *Physical Review Accelerators and Beams* **21**, 102002 (2018).
- [19] A. Cahill, J. Rosenzweig, V. Dolgashev, Z. Li, S. Tantawi, and S. Weathersby, *Physical Review Accelerators and Beams* **21**, 061301 (2018).
- [20] G. Reuter and E. Sondheimer, *Proceedings of the Royal*

- Society of London. Series A. Mathematical and Physical Sciences **195**, 336 (1948).
- [21] R. A. Matula, Journal of Physical and Chemical Reference Data **8**, 1147 (1979).
- [22] G. Stupakov, K. Bane, P. Emma, and B. Podobedov, Physical Review Special Topics-Accelerators and Beams **18**, 034402 (2015).
- [23] S. Tantawi, M. Nasr, Z. Li, C. Limborg, and P. Borchard, Physical Review Accelerators and Beams **23**, 092001 (2020).
- [24] J. Wang, *Accelerator structure development for NLC/GLC*, Tech. Rep. (Stanford Linear Accelerator Center, Menlo Park, CA (US), 2004).
- [25] S. G. Tantawi, C. D. Nantista, V. A. Dolgashev, C. Pearson, J. Nelson, K. Jobe, J. Chan, K. Fant, J. Frisch, and D. Atkinson, Physical Review Special Topics-Accelerators and Beams **8**, 042002 (2005).
- [26] F. Nix and D. MacNair, Physical Review **60**, 597 (1941).
- [27] D. Kajfez, IEEE transactions on microwave theory and techniques **42**, 1149 (1994).
- [28] T. P. Wangler, *RF Linear accelerators, Chapter 5* (John Wiley & Sons, 2008).
- [29] K. L. Bane, T. L. Barklow, M. Breidenbach, C. P. Burkhardt, E. A. Fauve, A. R. Gold, V. Heloin, Z. Li, E. A. Nanni, M. Nasr, *et al.*, arXiv preprint arXiv:1807.10195 (2018).
- [30] J. Rosenzweig, B. Carlsten, F. Krawczyk, J. Lewellan, E. Simakov, B. Spataro, T. Abe, V. Shiltsev, N. Solyak, and A. White, .
- [31] J. Rosenzweig, N. Majernik, R. Robles, G. Andonian, O. Camacho, A. Fukasawa, A. Kogar, G. Lawler, J. Miao, P. Musumeci, *et al.*, New Journal of Physics **22** (2020).